Collisions among elongated settling particles: The twofold role of turbulence

(article starts on next page)

Collisions among elongated settling particles: The twofold role of turbulence

Anđela Grujić ✉ ; Akshay Bhatnagar (अक्षय भटनागर) ; Gaetano Sardina ; Luca Brandt

Check for updates

CrossMark

View Online

Export Citation

Physics of Fluids

Special Topic:
Flow and Civil Structures

Submit Today

AIP Publishing

AIP Publishing

Collisions among elongated settling particles: The twofold role of turbulence ⓔⓟ

View Online   Export Citation   CrossMark

Anđela Grujić,[1,a)] ⓘⒹ Akshay Bhatnagar (अक्षय भटनागर),[1,2] ⓘⒹ Gaetano Sardina,[3] ⓘⒹ and Luca Brandt[1,4] ⓘⒹ

AFFILIATIONS

[1]SeRC (Swedish e-Science Research Centre) and FLOW, Department of Engineering Mechanics, KTH, SE-10044 Stockholm, Sweden
[2]Department of Physics, Indian Institute of Technology Palakkad, Palakkad 678 557, India
[3]Department of Mechanical and Maritime Sciences, Chalmers University of Technology, 412 96 Gothenburg, Sweden
[4]Department of Energy and Process Engineering, Norwegian University of Science and Technology (NTNU), Trondheim, Norway

[a)]Author to whom correspondence should be addressed: andelag@mech.kth.se

ABSTRACT

We study the collision rates of settling spheres and elongated spheroids in homogeneous, isotropic turbulence by means of direct numerical simulations aiming to understand microscale-particle encounters in oceans and lakes. We explore a range of aspect ratios and sizes relevant to the dynamics of plankton and microplastics in water environments. The results presented here confirm that collision rates between elongated particles in a quiescent fluid are more frequent than those among spherical particles in turbulence due to oblique settling. We also demonstrate that turbulence generally enhances collisions among elongated particles as compared to those expected for a random distribution of the same particles settling in a quiescent fluid, although we also find a decrease in collision rates in turbulence for particles of the highest density and moderate aspect ratios ($\mathscr{A} = 5$). The increase in the collision rate due to turbulence is found to quickly decrease with aspect ratio, reach a minimum for aspect ratios approximately equal to 5, and then slowly increase again, with an increase up to 50% for the largest aspect ratios investigated. This non-monotonic trend is explained as the result of two competing effects: the increase in the surface area with aspect ratio (beneficial to increase encounter rates) and the alignment of nearby prolate particles in turbulence (reducing the probability of collision). Turbulence mixing is, therefore, partially balanced by rod alignment at high particle aspect ratios.

I. INTRODUCTION

Particles suspended in a fluid play an important role in many industrial and natural processes.[1,2] Some of the examples are aerosol dispersion, transport of sediment in the estuaries and lakes, pulverized coal combustion, agglomeration of fine powders in gas flows, pneumatic conveying, water droplets in clouds, volcano eruptions, marine snow, and microplastics in oceans.[3–6] Often, these suspended particles collide and merge to form large aggregates. Understanding the process of collisions in the particle suspensions is necessary to predict the fate of the system. In most situations, the flow of the carrier fluid is turbulent and the chaotic turbulent velocities play an important role in the collision process. Due to density contrast, particles commonly settle with the settling affecting the collision rate between the particles.[4]

The present work is motivated by the need to understand microplastics fate in oceans. Plastics provide a lightweight, durable and hygienic surface for packaging.[7] However, its extensive use and our social behavior have led to the accumulation of solid plastic waste around marine areas.[8] Marine plastic litter has become a major concern and threat to the ecosystem and human health. Microplastic particles are found everywhere, in all marine environments in different densities, shapes and sizes.[9] Their properties change with the time spent in the marine eco-system due to mechanical degradation, biofouling, weathering and several other external factors.[10,11] The collision dynamics between microplastics, plankton, and marine microorganisms, can lead to the formation of polluted marine snow. Therefore, marine snow generation has an important role in the biogeochemical processing of microplastic pollution.[12,13] As a result of these different interactions, it is hard to predict the microplastics transport, behavior, migration, and other characteristics.[14] Nevertheless, we need to improve our current modeling capabilities as microplastics must be considered as a new kind of pollutant.

The dynamics of a microplastic particle differs from those of a passive tracer due to its shape and settling.[11] From the point of view of fluid dynamics, it can be argued that their dynamics are similar to sediment

grains, marine snow, and phytoplankton. In particular, a non-spherical shape is associated with a settling velocity not necessarily parallel to gravity and particle rotation induced by the local velocity gradients.

Phytoplankton is the most important and largest group of photosynthetic organisms in a coastal environment. They serve as the base of several food webs and play a crucial role in the carbon cycle of aquatic ecosystems.[15–17] These unicellular micro-organisms often form long chains, colonies, and filaments. These formations can be modeled as elongated particles in a turbulent flow, as microplastics. Some groups of phytoplankton are non-motile, and some of them have a siliceous cell wall that is denser than the seawater;[18] hence, they settle under gravity. Sedimentation of these organisms affects the trapping of CO_2 from the atmosphere into the ocean and how this is kept suspended there for a long time.[15,17] Collisions of spherical tracers and heavy inertial particles suspended in homogeneous and isotropic turbulence have been studied extensively in the literature. Tracer particles move with the local flow velocity and collide due to their finite size so that their mean collision rate depends on their size, the viscosity of the carrier fluid, and the mean rate of energy dissipation of the turbulence.[19] Heavy infinitesimal particles, instead, detach from the flow streamlines due to their inertia, which may lead to collisions characterized by a high relative velocity.[20,21] In the limit of high inertia, and high-density ratios, the collision rate is studied in Refs. 4 and 22.

As mentioned above, the settling velocity of an elongated particle depends on its orientation.[23–27] The interactions between elongated settling particles and turbulence have been studied, among others in Ref. 16, which provide evidence of the accumulation of elongated particles. Two elongated particles settling in a quiescent fluid with the same orientation have the same settling velocity and never collide. Differences in the orientation, however, will lead to a difference in their settling velocities which may lead to a collision, unlike the case of spherical particles. Collision rates of the ellipsoids settling in a quiescent fluid have been studied by Słomka and Stocker.[28] More recently, Arguedas-Leiva et al.[29] have studied the effect of elongation of the encounter rates of phytoplankton in turbulent flows. These authors have explored a parameter range going from a turbulence-dominated regime, when the settling speed is smaller than the turbulence fluctuations, to a settling-dominated regime, when turbulence weakly affects the particle settling. Here, we explore a range of settling speeds and aspect ratios that is relevant for the microplastics and phytoplankton in a marine environment and, therefore, focus on an intermediate regime where the effects of settling and turbulence are of similar order.[30]

Our analysis is based on the results of simulations of settling inertialess prolate spheroids in homogeneous isotropic turbulence (HIT). These settling spheroids weakly cluster in turbulent flows, which can lead to enhanced collision rates. The other quantity that determines the collision rate of the particles is their relative velocity. In this paper, we will, therefore, examine both aspects, the clustering and the relative velocity of settling inertia-less prolate spheroids in laminar and turbulent flows.

The paper is organized as follows. We begin by introducing the model used to describe the motion of inertialess ellipsoids in homogeneous isotropic turbulence in Sec. II. In Sec. III, we introduce the simulation parameters. Next, we investigate whether turbulence affects the collision rates of these particles and how this varies as a function of aspect ratio, settling speed and density ratio, see Sec. IV. The clustering and relative velocity are considered in this section. The main conclusions from this study are summarized in Sec. V.

II. GOVERNING EQUATIONS AND NUMERICAL METHOD

A. Fluid flow

The motion of the fluid is governed by incompressible Navier–Stokes equations, written here in dimensionless form,

$$\frac{\partial \boldsymbol{u}}{\partial t} + \boldsymbol{u} \cdot \nabla \boldsymbol{u} = -\nabla p + \frac{1}{Re}\nabla^2 \boldsymbol{u} + \boldsymbol{f}, \tag{1}$$

$$\nabla \cdot \boldsymbol{u} = 0, \tag{2}$$

where $\boldsymbol{u}$ is the velocity vector of the fluid at position $\boldsymbol{x}$ and time t, p is pressure, and $\boldsymbol{f}$ is the external forcing that supplies the energy to maintain the turbulence. $Re = UL/\nu$ is the Reynolds number of the flow, where, U, L, and ν denote the velocity scale, length scale, and kinematic viscosity of the fluid.

Equations (1) and (2) are numerically solved by a pseudo-spectral method with the 2/3 dealiasing rule. The third-order Runge–Kutta method is used for the time integration.[31] All the simulations are performed in a cubic box of length 2π with periodic boundary conditions in all three directions. The simulation box is discretized with 128^3 uniformly spaced points. To maintain a turbulent flow, we use a stochastic forcing $\boldsymbol{f}$ in Fourier space that acts isotropically on the first shell of wave vectors. The forcing amplitude is constant and the phase is delta-correlated in time.[32] The same numerical code has been used to study the clustering and sedimentation of inertia-less prolate spheroids with application to phytoplankton,[16] gyrotactic micro-organisms,[33] and rain droplet evaporation in clouds,[34] all in homogeneous isotropic turbulence.

The homogeneous and isotropic turbulent flow is defined by the Taylor microscale Reynolds number, $Re_\lambda = \frac{u'\lambda}{\nu}$, where u' is the root mean square of the velocity fluctuations, and $\lambda = \sqrt{\frac{\epsilon}{15\nu u'^2}}$ is the Taylor scale, with ϵ the mean rate of energy dissipation of the flow. For the simulations presented in this study, $Re_\lambda = 75$.

B. Particle motion

The elongated spheroids studied here are small when compared to the smallest turbulent eddies, hence smaller than the Kolmogorov length scale $\eta = (\nu^3/\epsilon)^{1/4}$ of turbulence. For the applications of this study, ϵ is chosen to correspond to the surface layer of the ocean, which is of the order $10^{-6}\,\mathrm{m^2/s^3}$, corresponding to a length scale $\eta = 1$ mm, while the particle density is assumed to be close to the density of the carrier fluid.[35]

The settling velocity of an ellipsoid in the Stokes flow depends on its orientation, defined here by the unit vector $\boldsymbol{p}$, and is given by the following expression:[23]

$$\boldsymbol{v}_s(\boldsymbol{p}) = \frac{1}{8\pi\mu l}(\beta_0 \boldsymbol{I} + \beta_1 \boldsymbol{pp}) \cdot \boldsymbol{g}, \tag{3}$$

where the dimensionless functions β_0 and β_1 are given by

$$\beta_0 = \frac{\mathscr{A}^2}{\mathscr{A}^2 - 1}(2\mathscr{A}^3 - 3\mathscr{A})\xi_+, \tag{4}$$

$$\beta_1 = \frac{-3\mathscr{A}^2}{\mathscr{A}^2 - 1} + 2\mathscr{A}\xi_+ + (\mathscr{A} - 2\mathscr{A}^3)\xi_-, \tag{5}$$

and the coefficients ξ_+ and ξ_-,

$$\xi_\pm = \frac{ln\left[\mathscr{A} \pm \sqrt{(\mathscr{A}^2 - 1)}\right]}{\sqrt[3]{\mathscr{A}^2 - 1}}. \quad (6)$$

In the above, μ is dynamic viscosity, $\boldsymbol{g}$ denotes the acceleration due to gravity, and $\mathscr{A}$ is the particle aspect ratio, i.e., the ratio between the length l and width w of the semi-major and semi-minor axis of a prolate. Equation (3) shows that the settling speed of a prolate spheroid depends on its orientation. The settling speed is maximum when its long side is aligned with gravity, and minimum when the long side is normal to the direction of gravity. Full expressions and explanations of the different functions of the aspect ratio $\mathscr{A}$ can be found, among others, in Ref. 27.

It may be convenient to rewrite Eq. (3) for the settling velocity $\boldsymbol{v}_s(\boldsymbol{p})$ as follows:

$$\boldsymbol{v}_s(\boldsymbol{p}) = v_{\min}\boldsymbol{e_g} + (v_{\max} - v_{\min})(\boldsymbol{e_g} \cdot \boldsymbol{p})\boldsymbol{p}, \quad (7)$$

where $\boldsymbol{e_g}$ is the unit vector in the direction of gravity, $v_{\min}$ and $v_{\max}$ are the minimum and maximum settling speeds of the particle. Combining Eqs. (3) and (7), it can be shown that

$$v_{\max} = \frac{\beta_0 + \beta_1}{8\pi\mu l}\Delta\rho g V, \quad (8)$$

$$v_{\min} = \beta_0 \frac{1}{8\pi\mu l}\Delta\rho g V, \quad (9)$$

where $\Delta\rho$ is the difference between the density of particle and fluid. We also define the average settling speed v_{avg} in a quiescent fluid as in Ref. 16

$$v_{\text{avg}} = \frac{v_{\max} + 2v_{\min}}{3}. \quad (10)$$

We assume that the microplastics and phytoplankton behave like passive tracers, as their densities are close to the density of the fluid[36] with their settling velocity given by Eq. (3). The translational motion of the particle is therefore governed by the following equation:

$$\frac{d\boldsymbol{x}}{dt} = \boldsymbol{u}|_x + \boldsymbol{v}_s(\boldsymbol{p}), \quad (11)$$

where $\boldsymbol{x}$ is the position of the particles, $\boldsymbol{u}|_x$ is fluid velocity at the position of the particle, the settling speed $\boldsymbol{v}_s(\boldsymbol{p})$ is given by Eq. (7), and $\boldsymbol{p}$ is the orientation vector introduced above.

It has been observed that the rotational relaxation times associated with spinning and tumbling of small prolate particles are small compared to the translational relaxation times;[37,38] we, therefore, use the inertialess equation for the rotational degrees of freedom.[39,40] The orientation vector $\boldsymbol{p}$ of an inertia-less spheroid particle obeys the Jeffery equation,[41]

$$\frac{d\boldsymbol{p}}{dt} = \frac{1}{2}\boldsymbol{\omega}|_x \times \boldsymbol{p} + \alpha[\boldsymbol{I} - \boldsymbol{pp}] \cdot \boldsymbol{E}|_x \cdot \boldsymbol{p}, \quad (12)$$

where $\boldsymbol{\omega}|_x$ is the flow vorticity at the particle's position, $\boldsymbol{I}$ the second-rank identity tensor, $\boldsymbol{E}|_x$ is the symmetric part of the velocity gradient tensor at the position of the particle, and α depends on the aspect ratio $\mathscr{A}\mathscr{R}$ of the particle,

$$\alpha = \frac{\mathscr{A}^2 - 1}{\mathscr{A}^2 + 1}. \quad (13)$$

To integrate the equations of motion for the particle [Eqs. (7) and (12)], we need flow velocity and its gradients at the position of the particle, which are obtained with second-order interpolation. The Runge–Kutta scheme used for the time advancement of the carrier phase has also been used to perform the time integration of the particle equations of motion. To track the orientation of the particle, we use a formulation based on quaternions (see Ref. 42).

III. SIMULATION PARAMETERS

To study encounter rates of elongated particles in turbulence and quiescent fluid, we consider prolate spheroids of aspect rations $\mathscr{A} = 1$ (spheres), 2, 5, 10, and 20. For each of the aspect ratios, we examine two different values of the dimensional average settling speeds, $v_{\text{avg}} = u_\eta$ and $v_{\text{avg}} = 3u_\eta$, where $u_\eta = (\nu\epsilon)^{1/4}$ is the Kolmogorov velocity of the underlying flow. Note again that there are no collisions among spheres of the same density in a quiescent environment as they all set with the same velocity, both in terms of magnitude and direction.

Table I reports the values of the maximum and minimum settling velocity that is used for the simulations with $v_{\text{avg}} = u_\eta$. When $v_{\text{avg}} = 3u_\eta$, all values from the Table I should be multiplied by 3, except for the ratio $v_{\max}/v_{\min}$ which is not changing with the absolute value of the settling speed. These velocities are presented in the SI units. To obtain these values from the dimensionless parameters used in the simulations, we have assumed a fluid density $\rho_{fl} = 1029\text{kg}/\text{m}^3$ and kinematic viscosity of the fluid $\nu = 10^{-6}\text{m}^2/\text{s}$ ($\varepsilon = 10^{-6}\text{W}/\text{kg}$ as mentioned above). These aim to represent a marine environment.

For the purpose of our analysis, that is comparing particles of different aspect ratio and same volume settling in a turbulent flow for the two values of the average settling speed mentioned above, we introduce the equivalent radius r_{eq}, defined so that the volume of a sphere with radius r_{eq} is equal to the volume V_{rod} of the elongated spheroids.

Furthermore, to analyze the effect of changing size and aspect ratio in a systematic way, we also fix the value of the average settling speed v_{avg} and vary separately the aspect $\mathscr{A}$ and particle size via r_{eq}. To have a constant settling speed while varying the particle volume and shape, we need to consider particles with different densities for each value of $\mathscr{A}$ and r_{eq}. The values of particle density ρ_p, corresponding to the different values of the aspect ratio $\mathscr{A}$ and of the equivalent diameter r_{eq} which give an average settling speed $v_{\text{avg}} = u_\eta$ and $3u_\eta$ are reported in Tables II and III in SI units. Not that with our choice of dimensional parameters the Kolmogorov velocity $u_\eta = 0.000\,93\,\text{m/s}$.

Note finally that we track 200 000 particles in each of the simulations, and save about 300 snapshots for each case, spaced in time by about one Kolmogorov timescale, to compute the statistics presented below. Particles are injected in fully developed homogeneous and isotropic turbulence. Since the particles under consideration behave

TABLE I. Maximum, minimum, and average of settling velocities for different values of the particle aspect ratios and settling speed equal to the Kolmogorov velocity of the underlying turbulence, $v_{\text{avg}} = u_\eta$.

$\mathscr{A}$	1	2	5	10	20
$v_{\max}\,(\text{m/s})$	0.000 93	0.001 02	0.001 11	0.001 17	0.001 21
$v_{\min}\,(\text{m/s})$	0.000 93	0.000 89	0.000 84	0.000 81	0.000 79
$v_{\max}/v_{\min}\,(-)$	1	1.145	1.328	1.440	1.526
$v_{\text{avg}}\,(\text{m/s})$	0.000 93	0.000 93	0.000 93	0.000 93	0.000 93

TABLE II. Densities of the particles in kg/m³ for different values of $\mathscr{A}$ and r_{eq} in μm to maintain a constant value of $v_{avg} = u_\eta$.

$r_{eq}(\mu m)$	$\mathscr{A}$				
	1	2	5	10	20
50	1205	1212.3	1248.44	1299.93	1379.35
75	1107.1	1110.47	1126.53	1149.42	1184.71
100	1072.97	1074.82	1083.86	1096.73	1116.59
125	1057.12	1058.33	1064.11	1072.35	1085.06
150	1048.52	1049.37	1053.38	1059.10	1067.93

TABLE III. Densities of the particles in kg/m³ for different values of $\mathscr{A}$ and r_{eq} in μm to maintain a constant value of $v_{avg} = 3u_\eta$.

$r_{eq}(\mu m)$	$\mathscr{A}$				
	1	2	5	10	20
75	1264.2	1275.27	1322.64	1391.54	1497.8
100	1161.3	1166.96	1194.17	1232.92	1292.7
125	1113.65	1117.3	1134.71	1159.51	1197.77
150	1087.78	1090.32	1102.41	1119.63	1146.21

FIG. 1. Visualization of elongated particles settling in homogeneous isotropic turbulence. The simulations track point particles (blue circle) and their orientation (indicated by the red arrows). Isocontours of the turbulent velocity magnitude are depicted on the background planes.

inertialess, they reach the statistical steady state rapidly. Convergence is checked comparing with the results obtained with half the samples.

IV. RESULTS

In our analysis, we first study the collision kernels, as obtained from the particle relative position. Afterward, we focus on the potential for particle clustering, and particles relative velocity at close distance. The results are based on the simulations introduced above, see the schematic visualization in Fig. 1, where we display the particle position $\boldsymbol{x}$ with blue dots and the orientation $\boldsymbol{p}$ with red arrows.
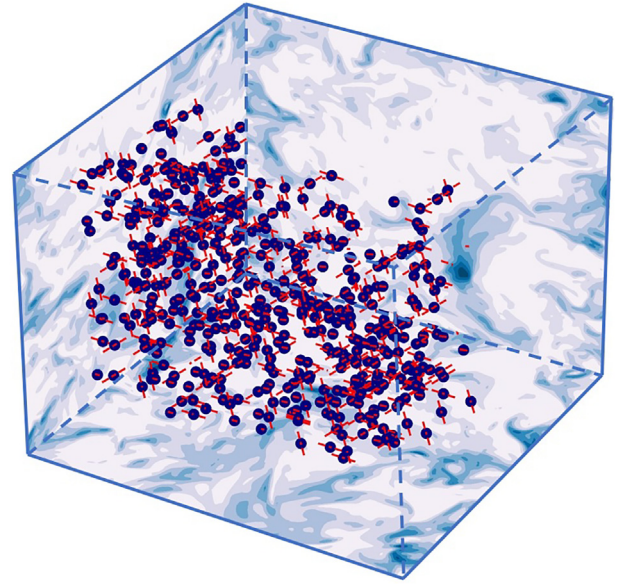
A. Collision kernel

1. Quiescent flow

An analytical expression for the collision kernel between thin cylindrical rods with spherical caps settling in a quiescent fluid is derived in Ref. 28. For our analysis, this is rewritten in terms of the quantities used here, r_{eq} and v_{avg}. Let us first introduce the coefficient $\boldsymbol{c} = \frac{\Delta\rho Vg}{\mu}$ as in Ref. 28 and combine it with Eqs. (10) and (7), such that

$$v_{avg} = \frac{2\beta_0 \Delta\rho Vg}{8\pi\mu l} + \frac{(\beta_0 + \beta_1)\Delta\rho Vg}{8\pi\mu l} = \frac{3\beta_0 + \beta_1}{24\pi l}\boldsymbol{c}.$$

From the equality $V_{rod} = V_{sp} = \frac{4}{3}\pi r_{eq}^3$, we obtain an expression for the length of the particle l, as function of r_{eq} and the aspect ratio $\mathscr{A}$. With this, the collision kernel for rods in quiescent Γ_q finally reads as

$$\Gamma_q = \frac{3v_{avg}\pi\beta_1 \left(\frac{16r_{eq}^3\mathscr{A}^2}{3 - \frac{1}{\mathscr{A}}}\right)^{2/3}}{2\mathscr{A}(3\beta_0 + \beta_1)}. \qquad (14)$$

The expression above is obtained assuming a uniform distribution for the orientation of rods of the same shape and density, see Ref. 28. This expression shows that the collision rate increases with the density contrast, the particle volume and aspect ratio, or simply—average settling velocity v_{avg}. When combining the expressions for the settling velocity Eqs. (7) and (14), at fixed volume V_{rod}, Γ_q displays a non-monotonic dependence on the aspect ratio $\mathscr{A}$. As example,[28] find that for $r_{eq} = 5$ μm, Γ_q is maximum at $\mathscr{A} \approx 50$.

To estimate the collision kernel in quiescent flow, we consider several snapshots of randomly distributed particles with random orientation vectors $\boldsymbol{p}$, following Ref. 28. The particles are assumed to keep their orientation in quiescent flow during the settling because we neglect the hydrodynamic interaction between them.

Collision rates between two populations of rods with orientations $\boldsymbol{p_1}$ and $\boldsymbol{p_2}$ can be calculated using the equation provided by[28]

$$\Gamma_{\boldsymbol{p_1},\boldsymbol{p_2}} = \frac{2l^2}{\mathscr{A}}\left(|\boldsymbol{p_1} \times \Delta\boldsymbol{v}| + |\boldsymbol{p_2} \times \Delta\boldsymbol{v}|\right). \qquad (15)$$

Here, $\boldsymbol{v_1}$ and $\boldsymbol{v_2}$ represent the velocities of the centers of mass of the particles, and $\Delta\boldsymbol{v} = \boldsymbol{v_1} - \boldsymbol{v_2}$ the relative velocity. The full collision kernel Γ is obtained by averaging $\Gamma_{\boldsymbol{p_1},\boldsymbol{p_2}}$ over all possible orientations $\boldsymbol{p_1}$ and $\boldsymbol{p_2}$. When the minimum distance between two particles is equal to the width of the particle w, as illustrated in Fig. 10 and described in the Appendix, the particles are considered to be in contact. To determine the collision kernel from our simulations, we calculate the average of $\Gamma_{\boldsymbol{p_1},\boldsymbol{p_2}}$ for all pairs of particles that have a minimum distance equal to w. In the appendix, we also show that the simulation data in quiescent flow correctly match the formula in Ref. 28.

Collision kernels in quiescent fluid are presented in Fig. 2, where we display values for different values of the settling speed (left and right columns), together with the values normalized with the collision
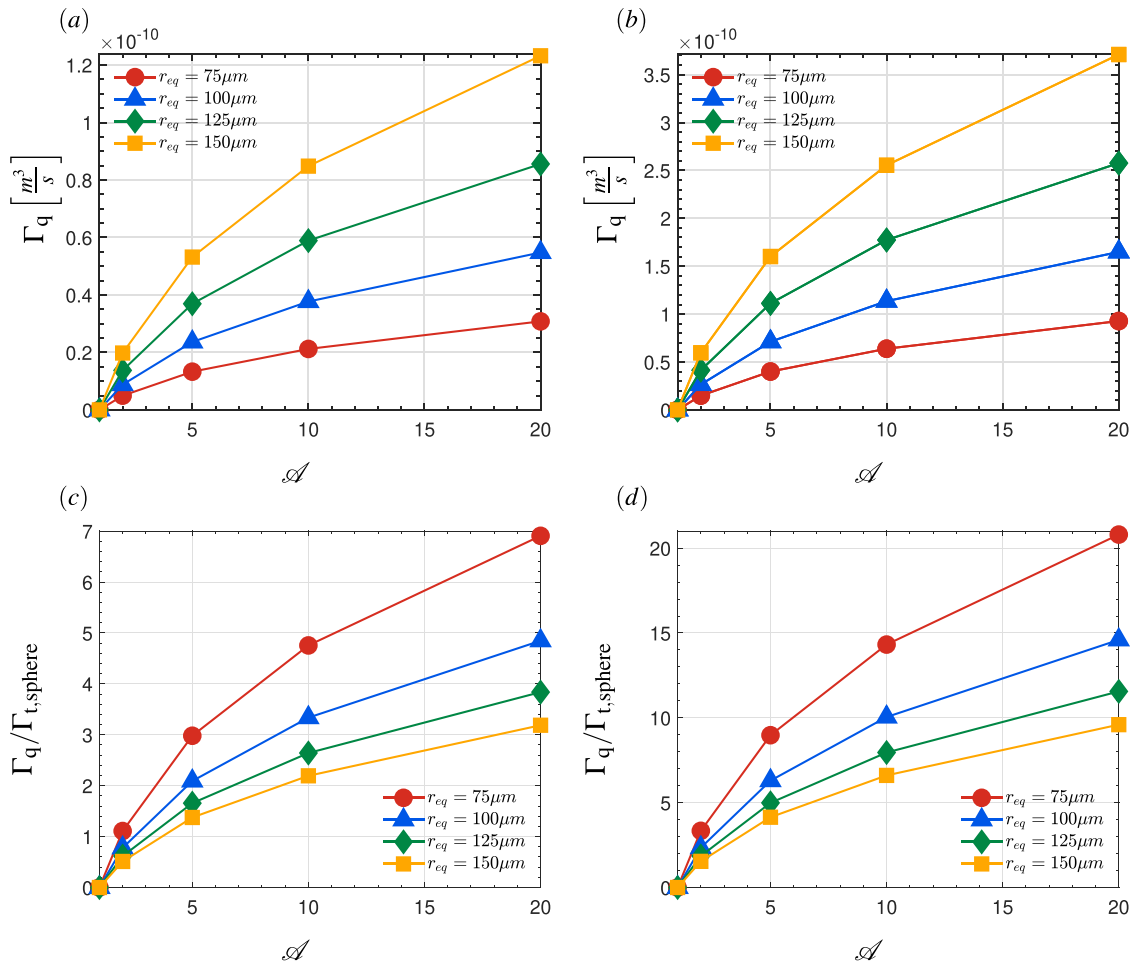
FIG. 2. (a) and (b) Collision kernel for cylinders with spherical caps in quiescent flow Γ_q as a function of the aspect ratio $\mathscr{A}$. (c) and (d) Ratio between the collision kernel of rods in quiescent flow Γ_q and neutrally buoyant spheres $\Gamma_{t,sphere}$ of the same volume in turbulent flow as a function of the aspect ratio $\mathscr{A}$, for the different values of particle volume, defined by the equivalent diameter r_{eq}, indicated in the legend. The data in panel (a) and (c) pertain to particles of different sizes and shapes with an average settling speed $v_{avg} = u_\eta$ and those in (b) and (d) to cases with $v_{avg} = 3u_\eta$, with u_η the Kolmogorov velocity of the underlying turbulence. Note that Γ_q is zero for spherical particles in quiescent flow, so that computations have actually been performed with a value $\mathscr{A} = 1.01$.

rates of spheres in turbulence (bottom row). These data are obtained from simulation statistics and are shown to match the theory, see the Appendix. The data in Fig. 2 show that for nearly spherical shapes ($\mathscr{A} = 1.01$), Γ_q is equal to zero, which confirms that there are no collisions between spheres in quiescent flow. The collision rates are found to increase with $\mathscr{A}$ and size of the particles; given the same settling speed, the increase with aspect ratio can be attributed to the increase in surface area for more elongated particles. Comparing panels a and b of Fig. 1, we notice the collision rates also increase at higher average settling speed, and the factor of increase is approximately 3, i.e., the ratio between the two settling speeds under examination.

As we will analyze the role of particle shape on the collision rates in turbulence, we introduce the ratio between the collision kernels of settling elongated particles in the quiescent fluid, Γ_q and the kernels for neutrally buoyant spheres in turbulence, $\Gamma_{t,sphere}$, where the latter is obtained from our simulations of nearly spherical particles, $\mathscr{A} = 1.01$, in homogeneous isotropic turbulence. The values of the ratio

$\Gamma_q/\Gamma_{t,sphere}$ are displayed in panels c and d of Fig. 2. We show these as a function of the particle aspect ratio $\mathscr{A}$ for the different particle volume and average settling speed under investigation. The data show that for $\mathscr{A} \geq 2$, Γ_q is larger than zero and this implies that settling rods in a quiescent flow have higher collision rates than neutrally buoyant spheres of the same volume transported in a turbulent flow. In particular, the collision rates increase by a factor approximately 20 for very elongated particles and average settling speeds equal to three times the Kolmogorov velocity scale. For nearly spherical shapes ($\mathscr{A} = 1.01$), when $\Gamma_q = 0$, we can appreciate the increase in collision rates due to turbulence.

2. Collisions in turbulence

Next, we turn our attention to the main objective of this work, i.e., the collision kernel of settling elongated particles in turbulent flows, denoted here by Γ_t.

02 February 2024 15:37:31

The collision rates in turbulence, Γ_t, are depicted as a function of the aspect ratio $\mathscr{A}$ in Figs. 3(a) and 3(b) for the two average settling speeds under investigation, $v_{avg} = u_\eta$ and $3u_\eta$ and for different particle volumes (see equivalent radius in the figure legend). The values of Γ_t are greater than 0 for all different particle sizes under investigation, i.e., for the different values of r_{eq}, and increase with the aspect ratio, $\mathscr{A} > 1$. Hence, in turbulence, the collision rates of settling rods are always greater than those between spherical particles of same volume and average settling speed. A comparison between the data in panels (a) and (b) indicates that the collision rates are higher for particles with $v_{avg} = 3u_\eta$ than for $v_{avg} = u_\eta$. The ratio between the two is less than 3. Indeed, we expect the collision rate to be proportional to the settling speed v_{avg} only when we are in the settling dominated regime,[29] as also shown above from the results in quiescent fluid. Quantitatively, we observe that the collision rates of settling rod-like particles are up to ten times higher than the collision rates of spheres with the same volume.

To obtain further insight on the role of turbulence, we compare the collision kernels of a suspension of settling rods in a quiescent fluid, denoted Γ_q, to those in the presence of turbulence, Γ_t, for the same monodisperse suspension. The ratio between the two, Γ_q/Γ_t, is displayed in panels (c) and (d) of Fig. 3. Note again that in a quiescent fluid there are no collisions among spheres because all particles just settle vertically and with same velocity (zero relative velocity), that is $\Gamma_q/\Gamma_t = 0$ for $\mathscr{A} = 1$.

The data in the figure reveal that for most of the values of $\mathscr{A}$ and r_{eq} the ratio Γ_q/Γ_t is smaller than 1, which implies that the collision rates of settling prolate particles increase in turbulence. This enhancement can be explained by a weak clustering, absent in quiescent fluid, and by the increase in the particle relative velocity, now induced by the turbulent fluctuations and not only by a different particle orientation (see discussion in Sec. IV B). The increase in collision rates between rods induced by the turbulence can reach up to 100% ($\Gamma_q/\Gamma_t \approx 0.5$). We also note that the difference between collision rates in quiescent
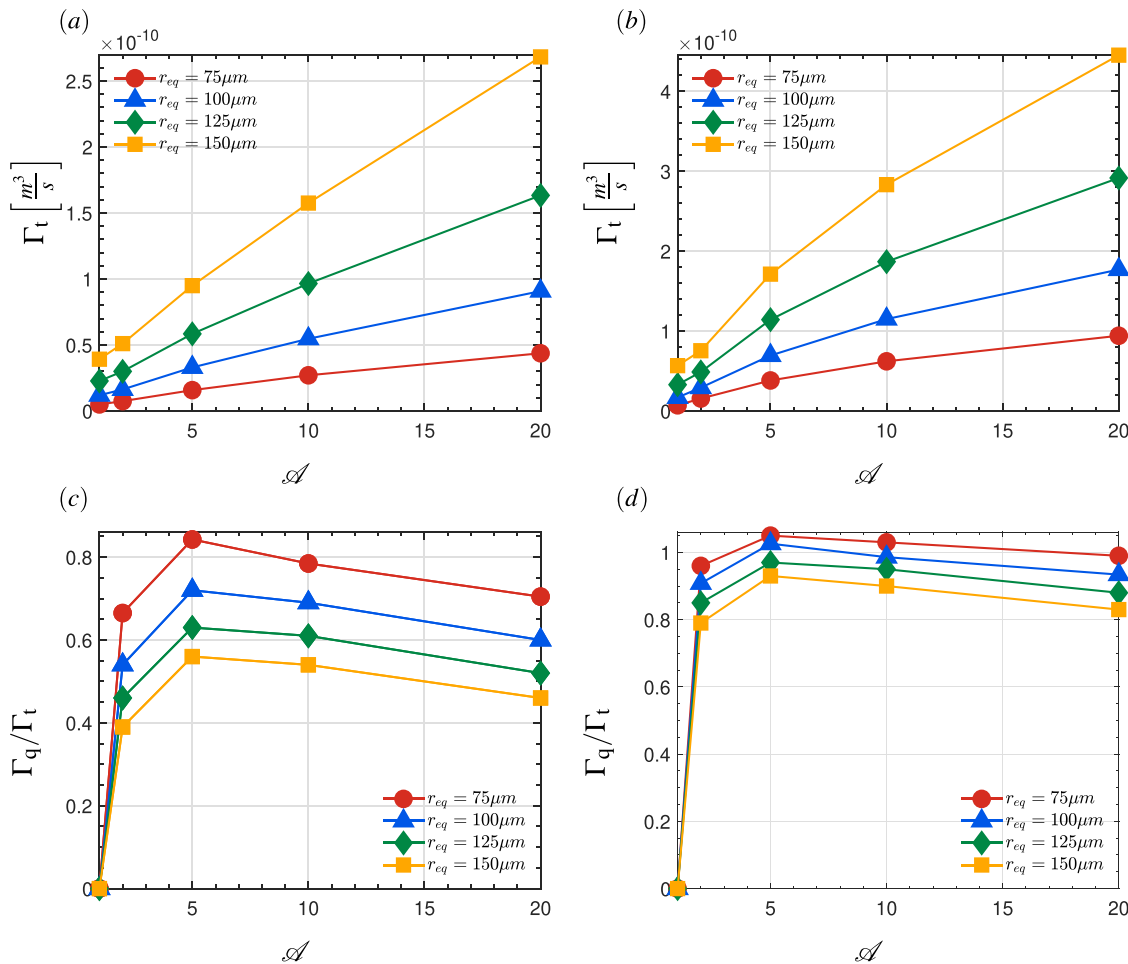

FIG. 3. (a) and (b) Collision kernel of cylinders with spherical caps in turbulence Γ_t as a function of the aspect ratio $\mathscr{A}$. (c) and (d) Ratio of collision kernels in quiescent fluid and turbulent flow Γ_q/Γ_t as a function of the aspect ratio $\mathscr{A}$. In all panels, the different curves pertain to different values of the particle volume, defined by the equivalent diameter r_{eq}, indicated in the legend. Panels (a) and (c) display the collision kernels for particles of average settling speed $v_{avg} = u_\eta$ whereas panels (b) and (d) those for particles with $v_{avg} = 3u_\eta$.

and turbulent flow is smaller for higher settling velocity and smaller particle sizes. Interestingly, we note a maximum of Γ_q/Γ_t for aspect ratios of approximately 5. For these intermediate values, the gain in turbulence is lower, and we even observe a reduction in collision rates in turbulence for the particles with the highest settling speed and $\mathscr{A} = 5$, see panel d) of Fig. 3. This is explained by the alignment between rods in turbulence, see Sec. IV B, which is not compensated by clustering and larger surface area as observed for higher values of $\mathscr{A}$.

Next, we wish to analyze collision kernels as a function of the particle density, which we have varied in order to fix the settling speed. To this end, we display the collision kernels from all our simulations in Fig. 4 vs the density ratio ρ_p/ρ_{fl}, see Table II. In particular, panel (a) depicts the collisions kernels in quiescent fluid, Γ_q, panel (b) those in turbulence, Γ_t, and panel (c) their ratio, Γ_q/Γ_t.

The data pertaining to settling in quiescent fluid confirm that the collision probability increases with settling speed and aspect ratio while decreasing in a notable manner with the density ratio. Note that a high-density ratio corresponds to a smaller particle size at the same settling speed. The overall picture is not different in turbulence flow, see panel (b) in Fig. 4; a remarkable difference is now the reduced difference for the two settling speeds under investigations (depicted with circles and squares). Finally, presenting the data in terms of relative variations shows that the increase in collision rates induced by turbulence is more limited for the high settling speed $v_{avg} = 3u_\eta$, i.e., $\Gamma_q/\Gamma_t > 0.8$ and almost independent of the density ratio. For the lower settling speed, $v_{avg} = u_\eta$, we notice a more clear increase in collision rates by the turbulence for increasing density ratios. Overall, the increase in collision rates in turbulence is strong for the smallest particles, and density ratios below 1.2.

To be able to better interpret the collision rate data just shown, we next focus on the potential for particle clustering, and on their relative velocity at close distance.

B. Particle clustering

To quantify the clustering of the settling particles, we compute the radial distribution function (RDF), which measures the probability of finding a particle pair separated by a given distance r, normalized by the value expected for uniformly distributed particles. The RDF is defined as

$$g(r) = \frac{1}{4\pi r^2}\frac{dN(r)}{dr}\frac{1}{n_0},\tag{16}$$

where $N(r)$ is the number of particle pairs having separation less than or equal to r and $n_0 = \frac{0.5N_p(N_p-1)}{V_0}$ is the mean number density of the pairs in the entire volume V_0 filled with N_p particles.

Figure 5 displays the radial distribution function g as a function of the pair separation r for settling speeds $v_{avg} = u_\eta$ and $3u_\eta$. The data show that for spheres, $\mathscr{A} = 1$, $g(r) \approx 1$ at all values of r/η, so no clustering is observed. For $\mathscr{A} > 1$, however, $g(r) > 1$ at small separations and decreases as r increases, approaching unity, the uniform distribution, for $r/\eta > 10$. The data, therefore, confirm a weak accumulation in turbulence for the case of elongated fibers. We note that the values of the radial distribution function increase with the aspect ratio $\mathscr{A}$ and the settling speed. As shown in Ardekani et al.,[16] a prolate spheroid has the tendency to preferentially sample a downwelling flow in a constant shear. Thus, the increase in settling speed observed in homogeneous and isotropic turbulence is solely attributed to this preferential sampling of regions exhibiting downwelling flow.

To focus on clustering, we display in Fig. 6 the values of the radial distribution function at contact, i.e., $g(r = 2r_{eq})$, vs the particle aspect ratio $\mathscr{A}$, for different values of the particle radius r_{eq}, as indicated in the legend, and for the two values of the settling speed considered (panel a and b for $v_{avg} = u_\eta$ and $v_{avg} = 3u_\eta$). For small separation distances,[43] estimated the radial distribution function of a monodisperse collection of inertial particles to be power-law function $g(r) = c_0 r^{-c_1}$, which is used here to obtain the values for distances approaching r_{eq}. The data in the figure reveal that the clustering increases with the aspect ratio, in agreement with the results in Ref. 16. Comparing the data in the two panels, we also observe that clustering in stronger for the largest settling speed examined, $v_{avg} = 3u_\eta$, than for particles with average settling speed $v_{avg} = u_\eta$. Finally, we note that, in all the cases examined here, clustering increases as r_{eq} is decreased, which is attributed to larger density of the smallest particles at the same settling speed, see Table II.

C. Particle mean relative velocity

Next, we examine the effect of aspect ratio $\mathscr{A}$ and particle size on the relative velocity between two particles at distance r; the value at a distance equal to the equivalent diameter, r_{eq}, is considered as this is
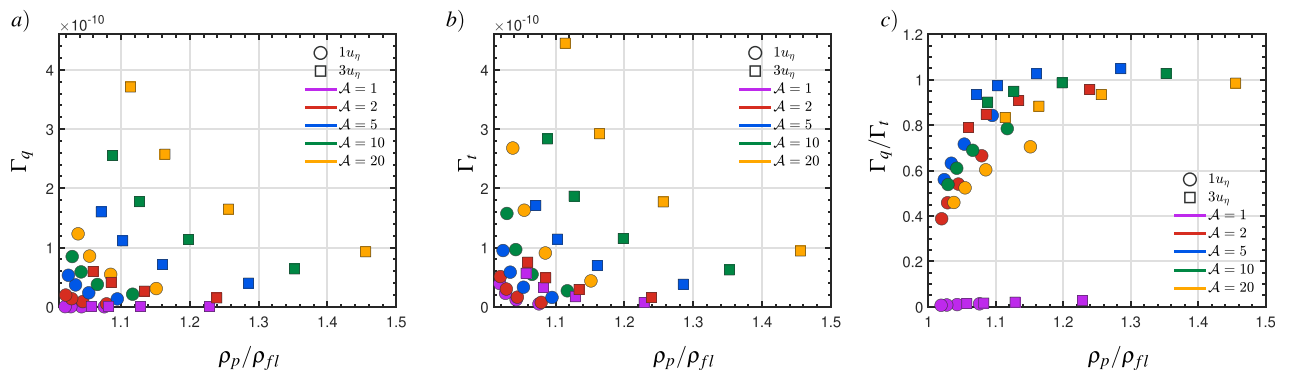

FIG. 4. Collision kernels vs the density ratio ρ_p/ρ_{fl} in (a) quiescent flow and (b) turbulence. Panel (c) shows the ratio of the two, Γ_q/Γ_t. Data from all simulations are displayed, with the color map indicating the aspect ratio and the symbols the settling speed: circle for $v_{avg} = u_\eta$, and squares for $v_{avg} = 3u_\eta$.

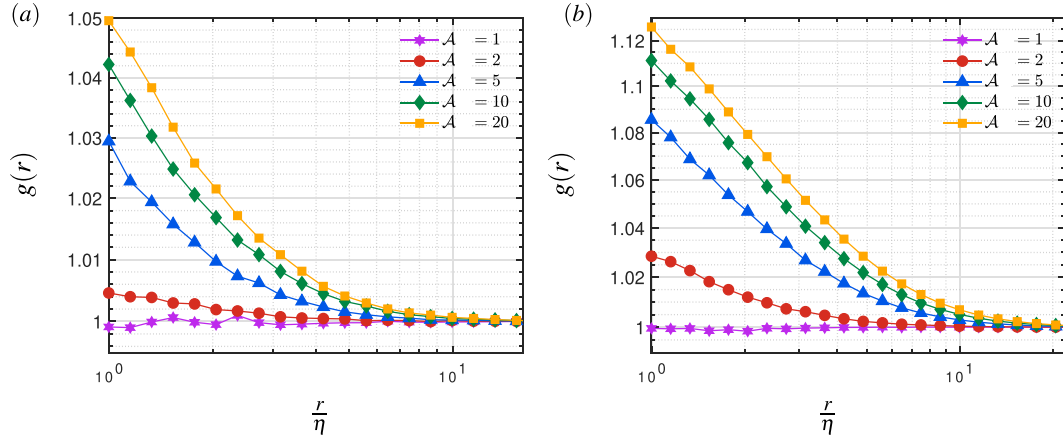**FIG. 5.** Radial distribution function vs the separation distance r for different values of the particle aspect ratio $\mathscr{A}$, see legend. Panel (a) displays values for a settling speed $v_{avg} = u_\eta$, whereas in (b), $v_{avg} = 3u_\eta$.

typically used to estimate the collision probability. Let us assume that two particles with separation r have velocity v_1 and v_2, and define the mean relative velocity as

$$dv^-(r) = -\langle (v_2 - v_1) \cdot \hat{r} \rangle_{app}, \tag{17}$$

where $\hat{r}$ is the unit vector along r and $\langle \rangle_{app}$ denotes the average taken over approaching pairs, i.e., with negative relative velocity.

The mean relative approaching velocity is displayed as a function of the separation r in Fig. 7 for $v_{avg} = u_\eta$ and $3u_\eta$. The magnitude of the relative velocity, dv^-, increase with r. Differences are found at small separation, and to be more pronounced for the largest settling speed under consideration. At large separation the curves approach a constant value, corresponding to the average fluctuation amplitude, i.e., the rms value of the underlying turbulence.

The relative velocity at contact, $dv^-(r_{eq})$, is displayed as a function of $\mathscr{A}$ for the average particle settling speed $v_{avg} = u_\eta$ in Fig. 8(a) and for $v_{avg} = 3u_\eta$ in panel 8(b). These values are normalized with the

values for spheres. The results show that the settling elongated particles have higher relative approaching velocities as compared to spheres with the same volumes and the values are greater for higher average particle settling speed $v_{avg} = 3u_\eta$. We also report data for different values of the particle volume, defined by means of the equivalent diameter r_{eq}, for each of the two average settling speeds under consideration. We note that values of the relative velocities are higher by a factor almost 3 for $v_{avg} = 3u_\eta$ than for particle settling with an average velocity $v_{avg} = u_\eta$. This suggests that the particle relative velocity at contact is more closely related to settling rather than to the local orientation and shear/vorticity.

Finally we investigate the average angle, θ, between the orientation vectors of two particles near contact, i.e., at a distance $\approx r_{eq}$ in turbulent flow. Figure 9 displays the average modulus of the cosine of the angle θ, $\langle |\cos(\theta)| \rangle$, as a function of the particle aspect ratio $\mathscr{A}$ and for the different values of r_{eq} under consideration. An average value $\langle |\cos(\theta)| \rangle \approx 0.5$ would be obtained if the orientation vectors are
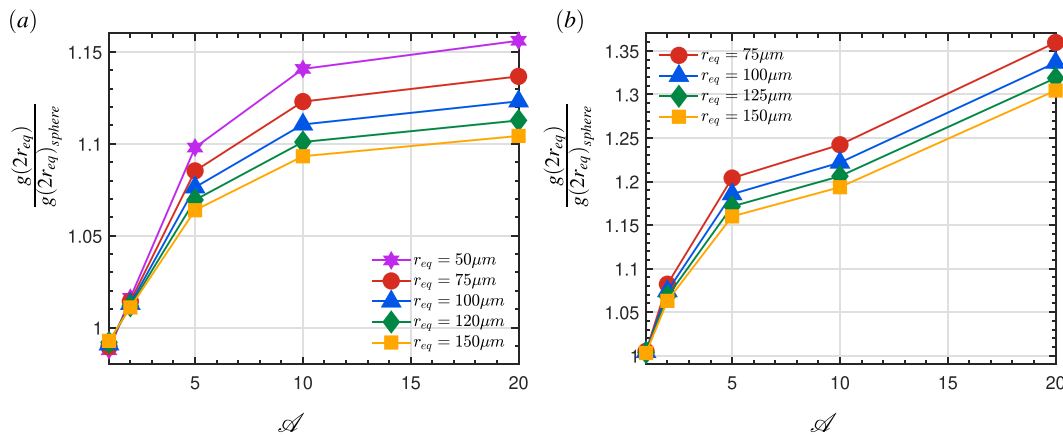

FIG. 6. Radial distribution function at contact $g(r = 2r_{eq})$, vs the particle aspect ratio $\mathscr{A}$ and for different values of the particle radius r_{eq}, see legend. Panel (a) displays values pertaining particles of same volume $(4/3\pi r_{eq}^3)$ and same settling speed $v_{avg} = u_\eta$ whereas in (b) $v_{avg} = 3u_\eta$. The values are normalized by the corresponding value for spherical particles.
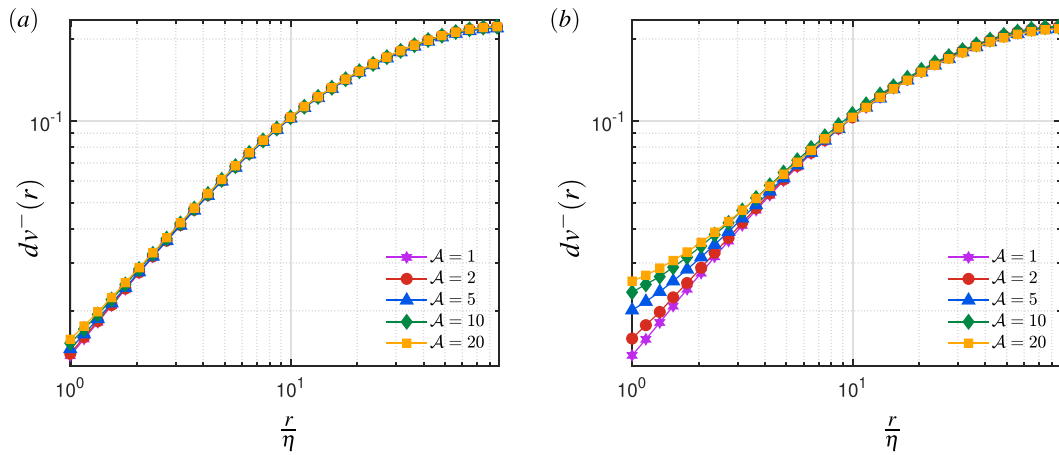
FIG. 7. Mean relative velocity $dv^-(r)$ vs the separation distance r for different values of the particle aspect ratio $\mathscr{A}$, see legend. Panel (a) displays values for settling speed $v_{avg} = u_\eta$ whereas in (b) $v_{avg} = 3u_\eta$.
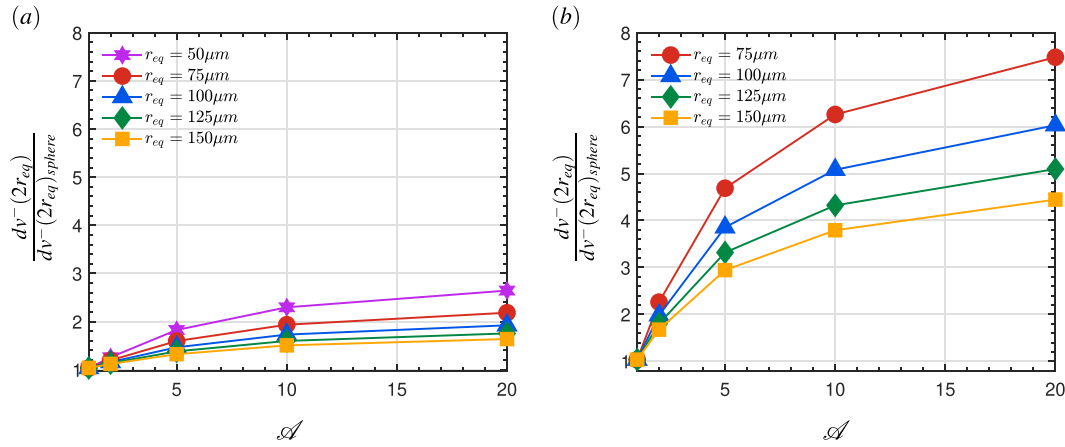

FIG. 8. Particle relative approaching velocities at contact, $dv^-(r_{eq})$ [see Eq. (17)] normalized by the value for spherical particles. The data are displayed as a function of the aspect ratio $\mathscr{A}$ for: (a) particle of fixed volume and average settling speed $v_{avg} = u_\eta$ and (b) $v_{avg} = 3u_\eta$. For each value of v_{avg}, data are shown for different values of the particle volume, defined through the equivalent diameter r_{eq}.

randomly distributed. Instead, we find here that for $\mathscr{A} > 1$, $\langle |\cos(\theta)| \rangle$ > 0.5. This indicates that, in the presence of turbulence, nearby particles tend to align with each other. As a consequence of this alignment, the particles have very similar settling directions, which leads to a decreasing collision probability. To conclude, we note that the alignment of the particle with the local velocity field has been investigated in several previous studies, see among others Marchioli *et al.*,[38] Parsheh *et al.*,[44] Meneveau[45] and the review by Voth and Soldati.[40] The anisotropic particle dynamics are significantly influenced by preferential alignment with the local velocity gradient tensor. This alignment not only greatly impacts particle rotations but also leads to instantaneous alignment among nearby particles. The study by Pumir and Wilkinson,[46] among others, highlights that thin elongated particles strongly align with the vorticity vector in isotropic turbulence, whereas alignment with the eigenvectors of the strain rate tensor is comparatively weaker.

V. CONCLUSION

We report the results of simulations of settling elongated spheroids with different aspect ratios in homogeneous, isotropic turbulence. The parameters used for the simulations are chosen to represent marine snow, diatoms, plankton, and microplastics (see Refs. 13 and 29) with settling velocities of the order of Kolmogorov velocities. To focus the analysis on particles of different shapes but the same volume and settling speed, we here adjust the particle density and simulate the settling of mono-disperse suspensions of prolate particles with an aspect ratio varying from 1 to 20 and settling speeds equal to 1 and 3 times the Kolmogorov speed of the underlying turbulence. The particle size is assumed to vary from 50 to $150\,\mu m$. Because of their small size, the particles have been assumed to behave like passive tracers with a correction given by the Stokes settling velocity—function of the orientation for non-spherical particles.
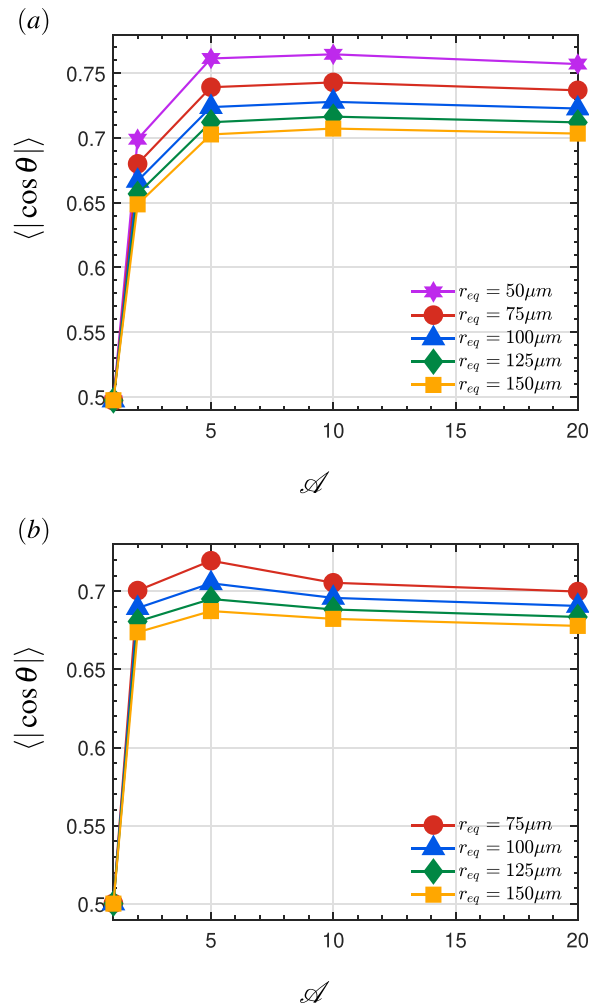
FIG. 9. Average of the modulus of the cosine of the angle between the orientation of particles at contact, $\langle |\cos (\theta)| \rangle$, as a function of aspect ratio $\mathscr{A}$ and for the different values of the particle volume, defined by the equivalent diameter r_{eq}, indicated in the legend. Panel (a) reports values for particle average settling speed $v_{avg} = u_\eta$, whereas in (b), $v_{avg} = 3u_\eta$.

From a methodological viewpoint, we introduce a computationally less expensive alternative for collision detection between rods. Specifically, we do not directly count collisions during the time integration of the governing equations but estimate the collision rate from the statistics of the minimum distance as function of relative position and orientation, in the limit of the distance between the surface going to zero. (See details in the manuscript Appendix where we validate the proposed approach.)

This work extends previous studies which have shown that collision rates between randomly oriented elongated particles settling in a quiescent fluid can be much larger than collision rates among spheres settling in homogeneous and isotropic turbulence.[28,29] This significant increase in collision rates is due to the oblique settling speed of elongated objects, in turn, a consequence of the drag-anisotropy in Stokes flows:[23] a random distribution of orientation would therefore lead to collisions

between rods even if they all have the same size and density. Moreover, numerical simulations and experiments have shown that elongated particles can cluster in a turbulent flow[16] and that collision rates increase with the aspect ratio of the elongated spheroids, the idealized shape usually assumed in theoretical and numerical models. This has been shown in the study by Arguedas-Leiva et al.[29] and confirmed by the analysis performed here for a wide range of parameters. We also recall, as known from several previous studies in different contexts, that turbulence significantly increases the collision rates of nearly spherical particles.

The new results presented here demonstrate that turbulence generally enhances collisions among elongated particles as compared to those expected for a random distribution of the same particles settling in a quiescent fluid. The increase in collision probability is much less pronounced than for nearly spherical particles, but still significant: For the cases considered in this study, this enhancement reaches up to 50% for very elongated particles. In particular, the increase in collision rate due to turbulence is found to quickly decrease with the aspect ratio, reach a minimum for aspect ratios approximately equal to 5, and then slowly increase again. Note that for $\mathscr{A} = 5$ we even find a lower collision probability in turbulence than in quiescent fluid for particles of highest density ratios (corresponding to settling speeds equal to three times the Kolmogorov velocity).

This non-monotonic trend is explained as the result of two competing effects: the increase in the surface area with aspect ratio (beneficial to increase encounters rates) and the alignment of nearby prolate particles in turbulence (reducing the probability of collision). Both effect are more pronounced when increasing the particle aspect ratio, with the former responsible for the increase observed at high aspect ratios despite the particle alignment, which becomes independent of the particle shape for $\mathscr{A} > 5$.

In addition, our simulations also show that the collision rates increase almost proportionally to the settling speed and the clustering due to the particle shape is relatively more important at a lower settling speed. Note finally that we have here considered collisions among particles of the same shape, size and density, while tiny particles dispersed in the ocean, either naturally or as a consequence of human activity, are characterized by a range of different settling speeds. In the future, it would therefore be relevant to investigate and estimate collision rates among particles with different densities, sizes and shapes.

AUTHOR DECLARATIONS
Conflict of Interest

The authors have no conflicts to disclose.

Author Contributions

The code has been developed by Gaetano Sardina (G.S.) and Anđela Grujić (A.G.). Simulations are performed by Anđela Grujić (A.G.). The paper is written by Anđela Grujić (A.G.) with feedback

02 February 2024 15:37:31

DATA AVAILABILITY

The data that support the findings of this study are available from the corresponding author upon reasonable request.

APPENDIX: COMPUTATION OF COLLISION KERNELS FROM DNS DATA

We present here an alternative approach to determine the collision kernel from point-particle simulations of rod-like particles in turbulent flows, which is computationally less expensive than counting directly the collisions during time integration. This is based on the estimation of the collision probability at distances approaching the distance between the rod surfaces at collision, i.e., the rod width w (see Fig. 10). We validate it by showing a good matching with the theory presented in Refs. 28 and 29 in quiescent fluid.

For the encounter detection algorithm, we approximate the particles as thin rods with spherical caps. The length of the rod is l, and the diameter is w; aspect ratio $\mathscr{A} = l/w$. The position of the center of mass is $\boldsymbol{x}$, and its axis is oriented along the direction defined by the unit vector $\boldsymbol{p}$. The coordinate of a point along its axis can be written in terms of the parameter t as

$$r(t) = \boldsymbol{x} + t\left(\frac{l}{2} - \frac{w}{2}\right)\boldsymbol{p}; \quad t \in [-1, 1],$$

$$= \boldsymbol{x} + t\left(1 - \frac{1}{\mathscr{A}}\right)\frac{l}{2}\boldsymbol{p}. \tag{A1}$$

Next, we consider two such rods having centers of mass at $\boldsymbol{x}_1$ and $\boldsymbol{x}_2$, separation $\Delta\boldsymbol{x} = \boldsymbol{x}_1 - \boldsymbol{x}_2$, and orientations along $\boldsymbol{p}_1$ and $\boldsymbol{p}_2$. Following Ref. 29, the minimum distance between the surface of the two is

$$r_{min} = \sqrt{\left[\frac{l}{2}\left(1 - \frac{1}{\mathscr{A}}\right)(\boldsymbol{p}_1 t_{min} - \boldsymbol{p}_2 s_{min}) + \Delta\boldsymbol{x}\right]^2}, \tag{A2}$$

where

$$t_{min} = \frac{2}{l(\mathscr{A}-1)}\frac{\mathscr{A}}{(\boldsymbol{p}_1 \cdot \boldsymbol{p}_2)^2 - 1}(\Delta\boldsymbol{x} \cdot \boldsymbol{p}_1 - (\boldsymbol{p}_1 \cdot \boldsymbol{p}_2)\Delta\boldsymbol{x} \cdot \boldsymbol{p}_2),$$

$$s_{min} = \frac{2}{l(\mathscr{A}-1)}\frac{\mathscr{A}}{(\boldsymbol{p}_1 \cdot \boldsymbol{p}_2)^2 - 1}((\boldsymbol{p}_1 \cdot \boldsymbol{p}_2)\Delta\boldsymbol{x} \cdot \boldsymbol{p}_1 - \Delta\boldsymbol{x} \cdot \boldsymbol{p}_2). \tag{A3}$$
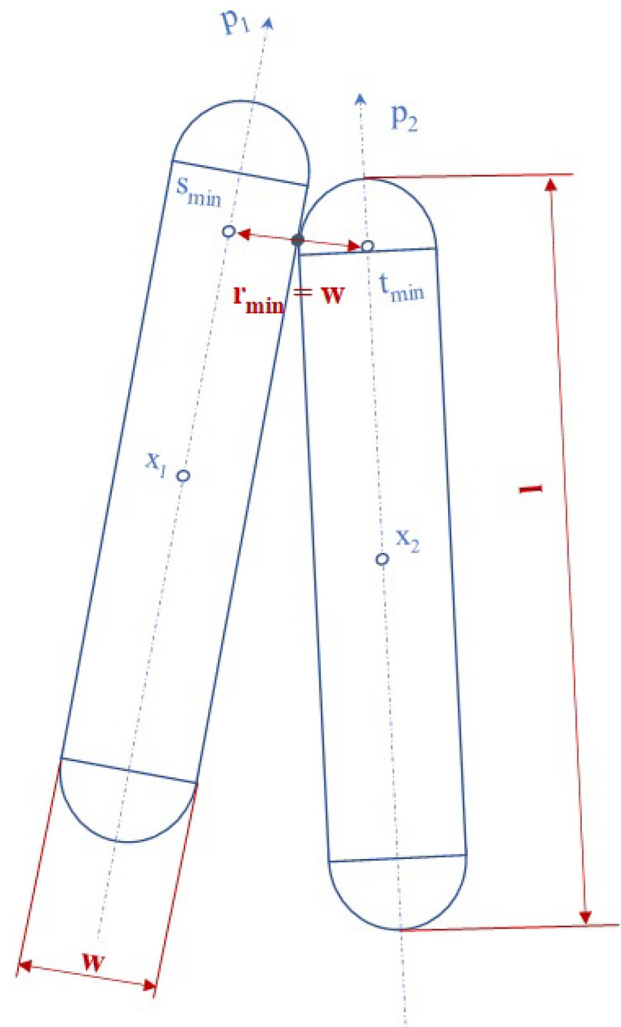

FIG. 10. Contact between two equal cylindrical rods with spherical caps. Definition of minimum distance r_{min}, t_{min}, and s_{min}, used to identify the particle relative position from their orientation and center of mass location. Contact occurs when $r_{min} = w$, the fiber cross section diameter.

The equations presented above give the minimum distance only when $-1 \le t_{min} \le 1$ and $-1 \le s_{min} \le 1$. If t_{min} or s_{min} lie outside the interval $[-1, 1]$, we should use the following expressions:

$$\text{set } t_{min} = -1 \text{ if } t_{min} < -1,$$
$$\text{set, } t_{min} = 1 \text{ if } t_{min} > 1,$$
$$\text{and } s_{min} = t_{min}\boldsymbol{p}_1 \cdot \boldsymbol{p}_2 + \frac{2}{l(\mathscr{A}-1)}\Delta\boldsymbol{x} \cdot \boldsymbol{p}_2. \tag{A4}$$

Similarly for s_{min},

$$\text{set } s_{min} = -1 \text{ if } s_{min} < -1,$$
$$\text{set } s_{min} = 1 \text{ if } s_{min} > 1,$$
$$t_{min} = s_{min}\boldsymbol{p}_1 \cdot \boldsymbol{p}_2 + \frac{2}{l(\mathscr{A}-1)}\Delta\boldsymbol{x} \cdot \boldsymbol{p}_1. \tag{A5}$$
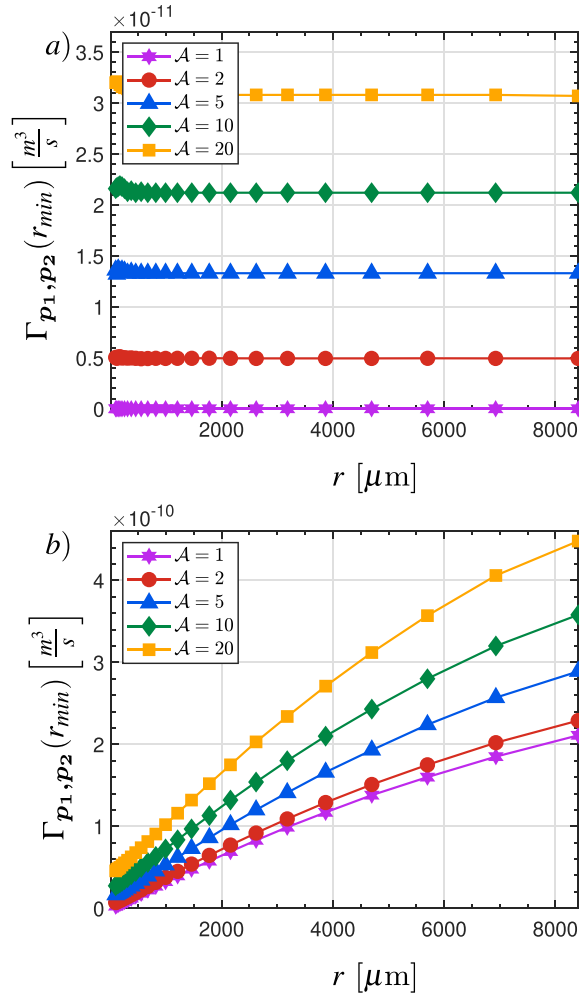
FIG. 11. Probability of minimum distance $\Gamma_{p_1,p_2}(r_{min})$ in (a) quiescent flow and (b) turbulent flow from the algorithm described in the appendix [Eq. (A6)] as a function of the distance between the particles, used to estimate the collision kernels presented in the main text. The figure reports values for the particle average settling speed $v_{avg} = u_\eta$.

FIG. 12. Collision kernel in quiescent flow from theory [Eq. (14)] and simulations as a function of aspect ratio $\mathscr{A}$ and for the equivalent radius of sphere $r_{eq} = 75(\mu\text{m})$. The figure reports values for the particle average settling speed $v_{avg} = u_\eta$. The data validate the algorithm presented in the Appendix.

The collision probability between non-spherical particles given by Eq. (15),[28] and reported here for clarity, is then evaluated as a function of the minimum distance r_{min}.

$$\Gamma_{p_1,p_2}(r_{min}) = \frac{2l^2}{\mathscr{A}} \left(|p_1 \times \Delta v| + |p_2 \times \Delta v| \right). \qquad (A6)$$

The collision kernel is finally estimated by extrapolating the values to the minimum possible separation w, the fiber diameter. The function $\Gamma_{p_1,p_2}(r_{min})$ is displayed in Fig. 11 for the case of settling fibers in quiescent and turbulent flow. In panel (a), the collision probability is independent of the particle–particle distance, as it should be for randomly oriented fibers in the absence of any flow (note that the oscillations at short distances are due to poor statistics in this range). For the case of turbulent flow, panel (b), we clearly identify an almost linear range for short separations, which validate the use
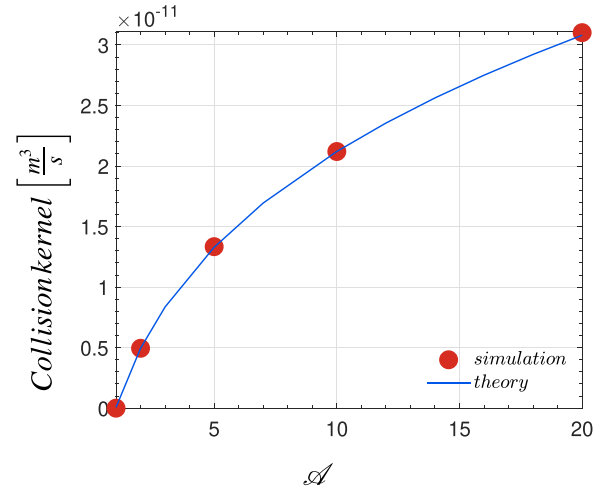
of linear extrapolation to the values of contact to estimate the collision kernels.

The algorithm used is therefore as follows:

1. Consider the particle pair defined by (x_1, p_1, v_1) and (x_2, p_2, v_1).
2. Calculate the vectors $\Delta x = x_1 - x_2$ and $\Delta v = v_1 - v_2$.
3. Calculate t_{min} and s_{min} using Eq. (A3).
4. If t_{min} and s_{min} lie outside of the interval $[-1, 1]$, use Eqs. (A4) and (A5).
5. Calculate r_{min} by using Eq. (A2).
6. Identify the bin corresponding to r_{min} in order to build a distribution of $\Gamma_{p_1,p_2}(r_{min})$.
7. Calculate Γ_{p_1,p_2} by using Eq. (15).
8. Add the value of Γ_{p_1,p_2} to the corresponding bin: $\Gamma(k) = \Gamma(k) + \Gamma_{p_1,p_2}$.
9. Repeat these steps for all particle pairs.

To validate our method, we report in Fig. 12 the collision kernel pertaining rod-like particles in quiescent flow as a function of the aspect ratio, for $v_{avg} = u_\eta$. The data from the simulations are compared with the theory, see Eq. (14), showing that the collision rates obtained by our method are in good agreement with the analytical model.

REFERENCES

[1] R. H. Davis and A. Acrivos, "Sedimentation of noncolloidal particles at low Reynolds numbers," Annu. Rev. Fluid Mech. **17**, 91–118 (1985).

[2] X. Cheng, Z. Cao, J. Li, and A. Borthwick, "A numerical study of the settling of non-spherical particles in quiescent water," Phys. Fluids **35**, 093310 (2023).

[3] E. Guazzelli, J. F. Morris, and S. Pic, *A Physical Introduction to Suspension Dynamics* (Cambridge University Press, 2011).

[4] G. Good, P. Ireland, G. Bewley, E. Bodenschatz, L. R. Collins, and Z. Warchaft, "Settling regimes of inertial particles in isotropic turbulence," J. Fluid Mech. **759**, R3 (2014).

[5]M. Filella, "Questions of size and numbers in environmental research on micro-plastics: Methodological and conceptual aspects," Environ. Chem. **12**, 527–538 (2015).

[6]A. J. K. Yang, J. Olsthoorn, and M.-L. Timmermans, "Sedimentation in particle-laden flows with and without velocity shear," Phys. Fluids **35**, 086604 (2023).

[7]J. N. Hahladakis, C. A. Velis, R. Weber, E. Iacovidou, and P. Purnell, "An overview of chemical additives present in plastics: Migration, release, fate and environmental impact during their use, disposal and recycling," J. Hazardous Mater. **344**, 179–199 (2018).

[8]O. Abayomi, P. Range, M. Al-Ghouti, J. Obbard, S. Almeer, and R. Ben-Hamadou, "Microplastics in coastal environments of the Arabian gulf," Mar. Pollut. Bull. **124**, 181 (2017).

[9]J. A. Ivar do Sul and M. F. Costa, "The present and future of microplastic pollution in the marine environment," Environ. Pollut. **185**, 352–364 (2014).

[10]A. Jahnke, H. P. H. Arp, B. I. Escher, B. Gewert, E. Gorokhova, D. Kühnel, M. Ogonowski, A. Potthoff, C. Rummel, M. Schmitt-Jansen, E. Toorman, and M. MacLeod, "Reducing uncertainty and confronting ignorance about the possible impacts of weathering plastic in the marine environment," Environ. Sci. Technol. Lett. **4**, 85–90 (2017).

[11]L. Khatmullina and I. Chubarenko, "Transport of marine microplastic particles: Why is it so difficult to predict?," Anthropocene Coasts **2**, 293–305 (2019).

[12]A. Porter, B. P. Lyons, T. S. Galloway, and C. Lewis, "Role of marine snows in microplastic fate and bioavailability," Environ. Sci. Technol. **52**, 7111–7119 (2018).

[13]M. Rahmani, A. Gupta, and L. Jofre, "Aggregation of microplastic and biogenic particles in upper-ocean turbulence," Int. J. Multiphase Flow **157**, 104253 (2022).

[14]M. S. Islam, M. M. Rahman, P. Larpruenrudee, A. Arsalanloo, H. M. Beni, M. A. Islam, Y. Gu, and E. Sauret, "How microplastics are transported and deposited in realistic upper airways?," Phys. Fluids **35**, 063319 (2023).

[15]N. Jiao, G. J. Herndl, D. A. Hansell, R. Benner, G. Kattner, S. W. Wilhelm, D. L. Kirchman, M. G. Weinbauer, T. Luo, F. Chen, and F. Azam, "Microbial production of recalcitrant dissolved organic matter: Long-term carbon storage in the global ocean," Nat. Rev. Microbiol. **8**, 593–599 (2010).

[16]M. Ardekani, G. Sardina, L. Brandt, L. Karp-Boss, R. Bearon, and E. Variano, "Sedimentation of inertia-less prolate spheroids in homogenous isotropic turbulence with application to non-motile phytoplankton," J. Fluid Mech. **831**, 655–674 (2017).

[17]W. Clifton, R. N. Bearon, and M. A. Bees, "Enhanced sedimentation of elongated plankton in simple flows," IMA J. Appl. Math. **83**, 743–766 (2018).

[18]R. W. Eppley, R. W. Holmes, and J. D. H. Strickland, "Sinking rates of marine phytoplankton measured with a fluorometer," J. Exp. Mar. Biol. Ecol. **1**, 191–208 (1967).

[19]P. G. Saffman and J. S. Turner, "On the collision of drops in turbulent clouds," J. Fluid Mech. **1**, 16–30 (1956).

[20]M. Wilkinson, B. Mehlig, and V. Bezuglyy, "Caustic activation of rain showers," Phys. Rev. Lett. **97**, 048501 (2006).

[21]A. Bhatnagar, K. Gustavsson, and D. Mitra, "Statistics of the relative velocity of particles in turbulent flows: Monodisperse particles," Phys. Rev. E **97**, 023105 (2018).

[22]J. Abrahamson, "Collision rates of small particles in a vigorously turbulent fluid," Chem. Eng. Sci. **30**, 1371–1379 (1975).

[23]J. Happel and H. Brenner, *Low Reynolds Number Hydrodynamics: With Special Applications to Particulate Media*, Prentice-Hall International Series in the Physical and Chemical Engineering Sciences (Prentice-Hall, 1965).

[24]D. L. Koch and E. S. G. Shaqfeh, "The instability of a dispersion of sedimenting spheroids," J. Fluid Mech. **209**, 521–542 (1989).

[25]M. R. Maxey, J. T. Stuart, and M. Tabor, "On the advection of spherical and non-spherical particles in a non-uniform flow," Philos. Trans. R. Soc. London, Ser. A **333**, 289–307 (1990).

[26]E. Krushkal and I. Gallily, "On the orientation distribution function of non-spherical aerosol particles in a general shear flow—II. The turbulent case," J. Aerosol Sci. **19**, 197–211 (1988).

[27]A. A. Dahlkild, "Finite wavelength selection for the linear instability of a suspension of settling spheroids," J. Fluid Mech. **689**, 183–202 (2011).

[28]J. Słomka and R. Stocker, "On the collision of rods in a quiescent fluid," Proc. Natl. Acad. Sci. U. S. A. **117**, 3372–3374 (2020).

[29]J.-A. Arguedas-Leiva, J. Słomka, C. C. Lalescu, R. Stocker, and M. Wilczek, "Elongation enhances encounter rates between phytoplankton in turbulence," Proc. Natl. Acad. Sci. U. S. A. **119**, e2203191119 (2022).

[30]J. Słomka, U. Alcolombri, F. Carrara, R. Foffi, F. J. Peaudecerf, M. Zbinden, and R. Stocker, "Encounter rates prime interactions between microorganisms," Interface Focus **13**, 20220059 (2023).

[31]R. Rogallo, "Numerical experiments in homogeneous turbulence," Report No. NASA-TM-81315 (NASA, 1981).

[32]A. Vincent and M. Meneguzzi, "Dynamics of vorticity tubes in homogeneous turbulence," J. Fluid Mech. **258**, 245–254 (1994).

[33]C. Zhan, G. Sardina, E. Lushi, and L. Brandt, "Accumulation of motile elongated micro-organisms in turbulence," J. Fluid Mech. **739**, 22–36 (2014).

[34]G. Sardina, F. Picano, L. Brandt, and R. Caballero, "Continuous growth of droplet size variance due to condensation in turbulent clouds," Phys. Rev. Lett. **115**, 184501 (2015).

[35]I. M. Susila, N. P. G. Suardana, C. I. P. K. Kencanawati, I. N. A. Thanaya, and I. W. B. Adnyana, "The effect of composition of plastic waste low density polyethylen (LDPE) with sand to pressure strength and density of sand/LDPE composites," IOP Conf. Ser.: Mater. Sci. Eng. **539**, 012043 (2019).

[36]D. Eerkes-Medrano, R. C. Thompson, and D. C. Aldridge, "Microplastics in freshwater systems: A review of the emerging threats, identification of knowledge gaps and prioritisation of research needs," Water Res. **75**, 63–82 (2015).

[37]L. Zhao, N. R. Challabotla, H. I. Andersson, and E. A. Variano, "Rotation of nonspherical particles in turbulent channel flow," Phys. Rev. Lett. **115**, 244501 (2015).

[38]C. Marchioli, L. Zhao, and H. I. Andersson, "On the relative rotational motion between rigid fibers and fluid in turbulent channel flow," Phys. Fluids **28**, 013301 (2016).

[39]M. Shin and D. L. Koch, "Rotational and translational dispersion of fibres in isotropic turbulent flows," J. Fluid Mech. **540**, 143–173 (2005).

[40]G. Voth and A. Soldati, "Anisotropic particles in turbulence," Annu. Rev. Fluid Mech. **49**, 249–276 (2017).

[41]G. B. Jeffery, "The motion of ellipsoidal particles immersed in a viscous fluid," Proc. R. Soc. London, Ser. A **102**, 161–179 (1922).

[42]M. P. Allen and D. J. Tildesley, *Computer Simulation of Liquids* (Oxford University Press, 2017).

[43]J. Chun, D. L. Koch, S. L. Rani, A. Ahluwalia, and L. R. Collins, "Clustering of aerosol particles in isotropic turbulence," J. Fluid Mech. **536**, 219–251 (2005).

[44]M. Parsheh, M. Brown, and C. Aidun, "Variation of fiber orientation in turbulent flow inside a planar contraction with different shapes," Int. J. Multiphase Flow **32**, 1354–1369 (2006).

[45]C. Meneveau, "Lagrangian dynamics and models of the velocity gradient tensor in turbulent flows," Annu. Rev. Fluid Mech. **43**, 219–245 (2011).

[46]A. Pumir and M. Wilkinson, "Orientation statistics of small particles in turbulence," New J. Phys. **13**, 093030 (2011).